



Formation and characterization of magnetron sputtered Ta–Si–N–O thin films

H. Yan^a, L. Li^a, F.Y. Ho^a, M.H. Liang^a, J.S. Pan^b, S. Xu^c, Z. Chen^{a,*}

^a School of Materials Science and Engineering, Nanyang Technological University, 50 Nanyang Avenue, 639798, Singapore

^b Institute of Material Research & Engineering, A*STAR (Agency for Science, Technology and Research), 3 Research Link, 117602, Singapore

^c Plasma Sources and Applications Center, NIE, Nanyang Technological University, 1 Nanyang Walk, 637616, Singapore

ARTICLE INFO

Available online 17 March 2009

Keywords:

Tantalum silicon nitride
Ta–Si–N–O film
Diffusion barrier coating
Magnetron sputtering
Thermal stability

ABSTRACT

Tantalum silicon nitride films have good potential to be used as hard coatings and diffusion barriers. In this work, films with different composition were deposited using a magnetron sputter under varying nitrogen flow rates. The composition, microstructure, thermal stability and electrical resistivity have been investigated. In the as-deposited state, all films consist of amorphous TaSi_xO_y, Ta_xO_y, Ta_xN_y and TaSi_x compounds. The composition of films is affected by N₂ flow rate. The resistivity of the as-deposited films increases with N concentrations. At elevated temperatures, all films show good thermal stability to at least 800 °C, while film with high Si concentration is largely amorphous at 900 °C because of highly stable TaSi_xO_y compounds. This study suggests that the TaSi_xO_y compounds could be the key factor in enhancing thermal stability of Ta–Si–N–O films.

© 2009 Elsevier B.V. All rights reserved.

1. Introduction

Ternary refractory metal Me–Si–N films (Me = Ti, Ta, W, Zr, V, Nb, Cr) have been widely explored for their excellent mechanical properties (e.g. superhardness). Large amount of work has been carried out since a decade ago on the microstructure and its correlation with hardness in these films [1–4]. The distinctive feature of metal nitride nanocrystals embedded in the amorphous silicon nitride matrix was identified as the microstructural reason for the achieved superhardness [5–7]. Thermal stability of the films is another important consideration since the coatings have to sustain high operating temperatures (e.g. coatings on cutting tools) without deteriorating the mechanical performance. For the same reasons, these films are therefore also potential candidates to be used as diffusion barriers in ultra-large-scaled-integrated (ULSI) circuit fabrication. In the semiconductor industry, copper has been widely used as interconnecting metal because of its low resistivity and good electron migration resistance compared to aluminum. However, copper is a faster diffuser in both Si and dielectric materials; and the fast diffusion may cause early breakdown of the devices. Therefore, a thin layer is usually deposited between the copper and dielectric layer to prevent copper diffusion. This layer must achieve 1) retardation of copper diffusion at elevated processing temperatures up to 400–500 °C; 2) good compatibility with copper and the dielectric materials; 3) high thermal stability; 4) relatively good conductivity. Bi-layer of Ta/TaN is commonly used nowadays as

copper diffusion barrier layer in the industry. However, the as-deposited TaN usually shows columnar polycrystalline structure. Due to this structure, diffusion along grain boundaries is very fast. As a result, TaN is not an ideal diffusion barrier. In order to maintain the continuous scaling down of integrated circuit, requirements of material behavior become increasingly stringent. Me–Si–N film is considered as a good candidate for a number of reasons, 1) the dense amorphous matrix eliminates the fast diffusion paths such as connected grain boundaries and dislocation pipes; 2) the high thermal stability implies that the microstructure of the films will not change during the ULSI device fabrication process; thus possible degradation of its barrier performance is unlikely.

While the most studied ternary barrier is Ti–Si–N films, such film deposited by a PVD process usually incorporates large amount of oxygen and effectively makes it a Ti–Si–N–O film [8–10]. To date, Ta–Si–N has received less attention, although theoretically it should be more stable than Ti–Si–N. Among the works reported so far, Lai [11] studied the influence of Ta/Si ratio on Ta–Si–N barrier performance.

Table 1
Parameters for magnetron sputtering film deposition.

Target power (W)	Ta: dc 200 W Si: rf 100 W
Base pressure (Torr)	4.0×10^{-6}
Working pressure (Torr)	7.5×10^{-3}
Gas flow rate (sccm)	Ar: 20 N ₂ : 3, 5, 8.5, 10
Process temperature	Room temperature
Film thickness (nm)	140 to 200

* Corresponding author.

E-mail address: aszchen@ntu.edu.sg (Z. Chen).

Table 2
The atomic composition of Ta–Si–N–O films according to the bonding orbital.

Specimen	N ₂ gas flow rate (sccm)	Ta (4f) (at.%)	Si (2p) (at.%)	N (1s) (at.%)	O (1s) (at.%)
N-3	3	33.3	14.2	6.1	46.4
N-5	5	38.0	13.7	10.6	38.0
N-8.5	8.5	36.7	12.5	12.6	36.7
N-10	10	42.9	12.7	8.6	42.9

He showed that a high Si content will increase the “degree of amorphization” for as-deposited Ta–Si–N barriers and proposed that the Ta/Si ratio should be optimized to avoid both Ta out-diffusion and Cu in-diffusion. Hubner et al. [12] investigated the influence of N content on the crystallization behavior of Ta–Si–N films. However, the exact chemical bonding state of elements in the film was not reported. In order to further understand the barrier performance and its thermal stability, a careful study of the deposition, phase composition, and the thermal stability of Ta–Si–N films is needed. Similar to the work on sputtered Ti–Si–N–O films, we found large amount of oxygen in the samples; therefore the films are more appropriately addressed as Ta–Si–N–O.

The current work investigated composition, microstructure, resistivity and thermal stability of Ta–Si–N–O films deposited by magnetron co-sputtering. In particular, chemical bonding conditions in the Ta–Si–N–O films were carefully studied by X-ray photoelectron spectroscopy (XPS). This work lays the foundation for future performance evaluation of this class of films either as a hard coating layer or diffusion barrier.

2. Experimental details

Ta–Si–N–O was formed by co-sputtering of Ta and Si targets with Ar and N₂ gas flow. P-type silicon wafers were used as the substrate. The silicon wafer was cut into pieces of 1 cm × 1 cm followed by chemical cleaning in the SC1 and SC2 solutions before being loaded into the magnetron sputter chamber. Ar flow rate was fixed at 20 sccm, while N₂ flow rate was varied from 3, 5, 8.5 to 10 sccm. Detailed deposition parameters are listed in Table 1. The samples are subsequently notated as N-3, N-5, N-8.5, and N-10 indicating the N₂ flow rate. To study the thermal stability of the films, samples were annealed in vacuum furnace for 60 min at temperatures from 400 °C to 900 °C.

The composition and chemical bonding states of all films were identified by X-ray photoelectron spectroscopy (XPS) using 1486.7 eV Al K_α irradiation. Surface layer stripping was carried out through in-situ sputtering inside XPS chamber before the XPS scan in order to

Table 4
Resistivity of the Ta–Si–N–O films before and after annealing.

Specimen	N ₂ gas flow rate (sccm)	Film composition	Resistivity, as-deposited (μΩ·cm)	Resistivity, annealing at 400 °C (μΩ·cm)	Resistivity, annealing at 800 °C (μΩ·cm)
N-3	3	Ta ₃₃₃ Si ₁₄ N ₆ O ₄₆	772	888	838
N-5	5	Ta ₃₈ Si ₁₄ N ₁₁ O ₃₈	1543	1786	2088
N-8.5	8.5	Ta ₃₆ Si ₁₂ N ₁₃ O ₃₇	19,760	48,625	89,667
N-10	10	Ta ₃₆ Si ₁₃ N ₉ O ₄₃	2171	2388	2276

eliminate the effect of surface oxidation. The atomic concentrations and bonding states of each element were determined using CASA-XPS package. The film thickness was measured using Alpha-Step 500 surface Profiler. The sheet resistance of films before and after annealing was measured using four point resistivity probe. Resistivity was calculated based on the measured film thickness and sheet resistance. Microstructure and crystallinity of the films was investigated by X-ray diffraction with a Rigaku™ XRD diffractometer using theta–2 theta mode at scan speed of 1° per minute. High resolution transmission electron microscopy was used to characterize the microstructure, in order to further substantiate the phase evolution at elevated temperatures.

3. Results and discussion

3.1. As-deposited Ta–Si–N–O films

Atomic concentration of the films at different N₂ flow rates is summarized in Table 2. It can be seen that as N₂ flow rate increases, atomic percentage of N in the film also increases until 8.5 sccm. An opposite trend was observed for Si concentration. High O concentration is observed for all as-deposited films. The oxygen in the film may be incorporated into the film from two sources. First, it could be due to the strong interaction between Ta and O ions from residues of O₂ and moisture (H₂O) inside the deposition chamber. Several elements such as Ti are known as oxygen getter [8,10,13] due to its strong affinity with oxygen. Similarly, Ta has strong affinity to oxygen as well. Second, the oxygen may also be introduced after the sputtering if porosity exists in the film. Del Re et al. [14] showed how the amount of oxygen in ZrN film was reduced from 32 to 2 at.% by applying a bias during film deposition. The bias plays the role of eliminating the porosity in the film, which can stop the oxygen from diffusing inside the film. While some amount of oxygen in the film is beneficial in terms of diffusion barrier performance [15], too much oxygen will harm the film conductivity. Therefore a balance has to be struck in the deposition of Cu diffusion barrier. Controlling the bias and deposition temperature can effectively control the oxygen content. In our current

Table 3
XPS binding energy peaks of each element with the area percentage of each peak and the represented bonding state.

N ₂ flow rate (sccm)	Ta			N		Si			O						
	Ta 4f7 BE	Area%	Bonding	N 1s BE	Area%	Bonding	Si 2p BE	Area%	Bonding	O 1s BE	Area%	Bonding			
3	22.5	13.2%	TaSi _x	396.7	100%	Ta _x N _y	98.6	8.3%	TaSi _x	530.6	37.5%	TaO _x			
	23.9	40.2%	Ta _x N _y , Ta _x O _y				102.5	91.8%	TaSiO _x				531.5	62.5%	TaSi _x O _y
	26.9	46.6%	TaSi _x O _y												
5	22.7	21.7%	TaSi _x	396.5	100%	Ta _x N _y	98.5	10.3%	TaSi _x	530.5	56.0%	TaO _x			
	24.4	39.0%	Ta _x N _y , Ta _y O _y				102.0	89.7%	TaSiO _x				531.2	44.0%	TaSi _x O _y
	26.6	39.3%	TaSi _x O _y												
	22.8	25.8%	TaSi _x												
8.5	24.4	40.9%	Ta _x N _y , Ta _x O _y	396.6	100%	Ta _x N _y	98.6	11.8%	TaSi _x	530.6	57.2%	TaO _x			
	26.7	33.3%	TaSi _x O _y				102.1	88.24%	TaSiO _x				531.3	42.8%	TaSi _x O _y
	22.9	20.3%	TaSi _x												
	24.6	38.1%	Ta _x N _y , Ta _x O _y												
10	22.9	20.3%	TaSi _x	396.5	100%	Ta _x N _y	98.7	9.8%	TaSi _x	530.7	52.0%	TaO _x			
	24.6	38.1%	Ta _x N _y , Ta _x O _y				102.4	90.2%	TaSiO _x				531.5	48.0%	TaSi _x O _y
	27.0	41.6%	TaSi _x O _y												

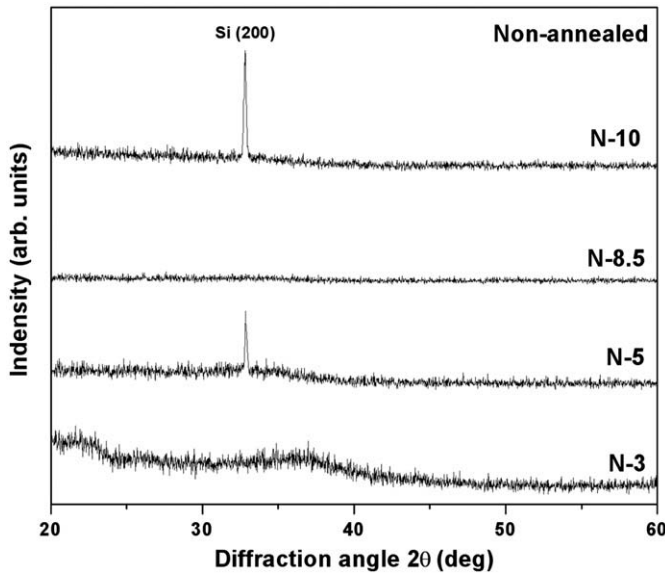


Fig. 1. XRD pattern of as-deposited Ta–Si–N–O films at different N_2 flow.

work, no bias was applied during the deposition, hence the high oxygen concentration.

A quantitative analysis of XPS spectra through peak fitting using CASA-XPS (Table 3) reveals the bonding states of all elements in different films. During the fitting of Ta 4f spectra, the 4f7 and 4f5 doublet peaks are constrained so that their area ratio is 4:3, and the separation is 1.9 eV. Therefore only Ta4f7 was used for the analysis. Three groups of Ta 4f binding energies were extracted from the fitting, including Ta 4f7 at 22.5–22.9 eV, 24.4–24.9 eV, and 26.6–27.0 eV. Among these groups, the Ta 4f7 at ~26.6 eV is usually referred as Ta_2O_5 , but it could be identified as tantalum silicate (Ta–Si–O) in which O is a linkage between Ta and Si [16]. Based on the study of Si 2p and O 1s spectra, it could be confirmed that this Ta 4f7 represents $TaSi_xO_y$. The existence of $TaSi_xO_y$ could be verified with Si 2p at 102.2 eV, and O 1s peak at 531.2 eV [17]. In all films, Si 2p peak at 102.0–102.5 eV and O 1s peak at 531.2–531.5 eV were observed. Therefore the simultaneous presence on the peaks of Ta 4f, Si 2p and O 1s suggests that $TaSi_xO_y$ exists in all as-deposited films. Another group of Ta 4f 7/2 peaks at 24.4–24.9 eV could be attributed to either Ta suboxide TaO_x or Ta_xN_y with different stoichiometry, such as 24.4 eV for Ta_3N_5 and 24.6 eV for TaN. Noticing that the FWHM of this peak is 2.71 eV, larger than that of 26.8 eV (1.30 eV), this peak could be the result of overlapping of Ta_xN_y and TaO_x . The existence of TaO_x is verified by the O 1s peak at 530.5–530.7 eV, while Ta_xN_y could be identified by N 1s peaks at 396.5–396.8 eV [18]. The third Ta4f 7 peak at ~22.7 eV could be identified as tantalum silicide, verified with Si 2p peak at 98.5–98.7 eV. There is no evidence of Si_3N_4 or SiO_2 formation. By the above XPS analysis, we conclude that the amorphous films consist of $TaSi_xO_y$, TaO_x , Ta_xN_y and $TaSi_x$ compounds. In the studied N_2 flow range, all samples are composed of this same group of compounds. However, the percentage of each compound varies with the N_2 flow. This is revealed by the peak area ratios of $TaSi_xO_y$: TaO_x and $TaSi_xO_y$: $TaSi_x$: they decrease as N_2 flow varies from 3 sccm to 8.5 sccm, then increase at 10 sccm. The same trend is observed for the Si concentration. The increasing $TaSi_xO_y$: $TaSi_x$ area ratio with Si content indicates that Ta silicate is preferred to Ta silicide with increasing Si content.

A relatively large variation in resistivity is observed for films with different composition, as shown in Table 4. The lowest resistivity measured was 772 $\mu\Omega$ cm, which is comparable with that of thin film TaN barrier. An increase of resistivity with N concentration is observed. It suggests that in order to obtain barrier films with low resistivity, N concentration should be kept low.

The XRD pattern of as-deposited films is shown in Fig. 1. All films are amorphous in the as-deposited state. The silicon substrate (200) peak is detected for some samples at 32.81° because of the deep X-ray penetration depth in the theta–2 theta detection mode. The appearance of the forbidden (200) peak was reported as a result of multiple diffraction effect [19].

3.2. Thermal stability of Ta–Si–N–O films

The resistivity after annealing at 400 and 800 °C is shown in Table 4. All films showed increased resistivity at 400 °C. Generally, samples N-3, N-5 and N-10 maintain relatively low resistivity in both the as-deposited and elevated temperatures. N-8.5 has higher resistivity in the as-deposited condition, and its resistivity further increases at the annealed temperatures. Since relatively low resistivity is a requirement for the barrier layer, N-8.5 composition may not be a suitable candidate for copper diffusion barrier application.

XRD patterns of samples N-3, N-5 and N-8.5 annealed at 400 °C, 800 °C and 900 °C for 60 min are shown in Fig. 2. Amorphous phases persist for all three samples at 400 °C and 800 °C. At 900 °C, Ta_2O_5 peaks are observed for all samples. It is also observed that, as N and Si contents increase, intensity of Ta_2O_5 peaks becomes higher. This coincides with the XPS result for as-deposited films that Ta_xO_y content increases at higher N content. This suggests that the crystalline Ta_2O_5 phase is formed mostly by crystallization of Ta_xO_y during deposition, rather than the decomposition of $TaSi_xO_y$. It should be noted that while N-5 and N-8.5 showed high crystalline content at 900 °C, N-3 remains largely amorphous. N-3 consists of a lower Ta and N content but a higher Si content compared to N-5 and N-8.5. The high $TaSi_xO_y$ / Ta_xN_y ratio means that the relative amount of the tantalum silicate is high. This suggests that with a moderate Si content, formation of Ta_xN_y and Ta_xO_y will be suppressed by the formation of $TaSi_xO_y$ which has higher thermal stability due to the complex bonding structure of silicate and heat absorption needed during decomposition of $TaSi_xO_y$.

High resolution TEM further confirms the crystallization behavior. Fig. 3(A) is the cross-section TEM image of sample after annealing at 800 °C, where no crystalline phase was observed. In Fig. 3(B), nanocrystals of the size of 3–5 nm are clearly seen embedded in the N8.5 film after 900 °C annealing. The TEM observation further confirms the XRD result indicating that nano-crystalline phase starts to form between 800 and 900 °C for most samples except N3.

4. Conclusion

Ta–Si–N–O films were deposited using a DC/RF magnetron sputter in this work. A considerable amount of oxygen concentration is detected for all samples. It is a result of strong oxygen affinity with Ta during the sputtering process. The as-deposited films are composed of amorphous $TaSi_xO_y$, Ta_xN_y , Ta_xO_y and $TaSi_x$. The elemental composition and their bonding states change with N_2 flow rate. Films with high Ta and O concentrations show high electrical resistivity. XRD study and resistivity measurement at elevated temperature show that thermal stability of films is affected by the compound composition. With Ta_2O_5 crystal found in other films at 900 °C, sample with high $TaSi_xO_y$ content remains largely amorphous. The high thermal stability and relatively low electrical resistivity suggest that Ta–Si–N–O films can be a good candidate for copper diffusion barrier films. The barrier performance can be improved by adjusting the composition to achieve high $TaSi_xO_y$ content.

Acknowledgement

Helpful discussion with, and suggestion from Prof. Stan Veprek and Dr. X. Z. Ding on the oxygen incorporation matter is gratefully acknowledged.

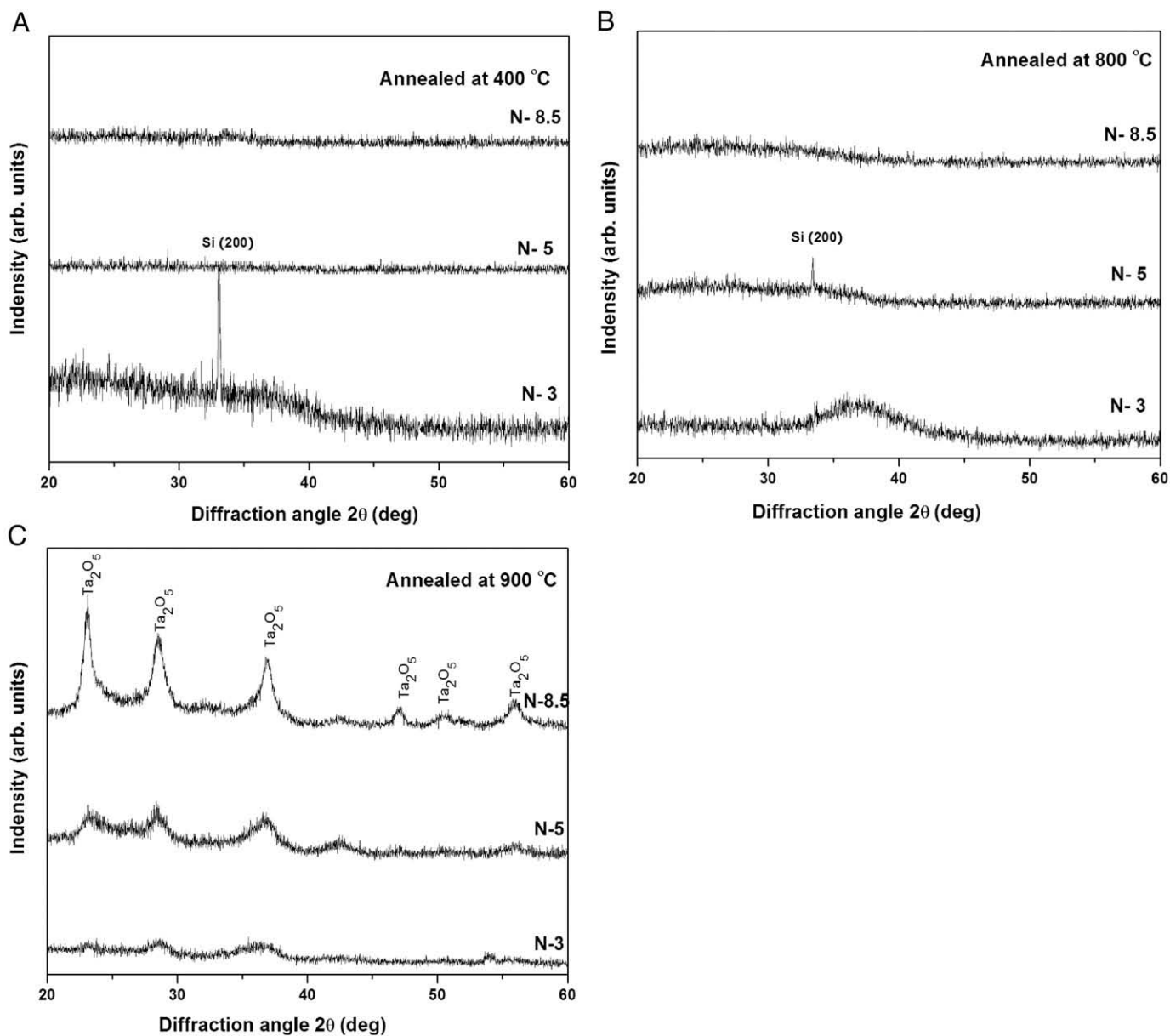


Fig. 2. XRD pattern evolution of sample N-3, N-5 and N-8.5 after annealed at (A) 400 °C, (B) 800 °C and (C) 900 °C for 60 min.

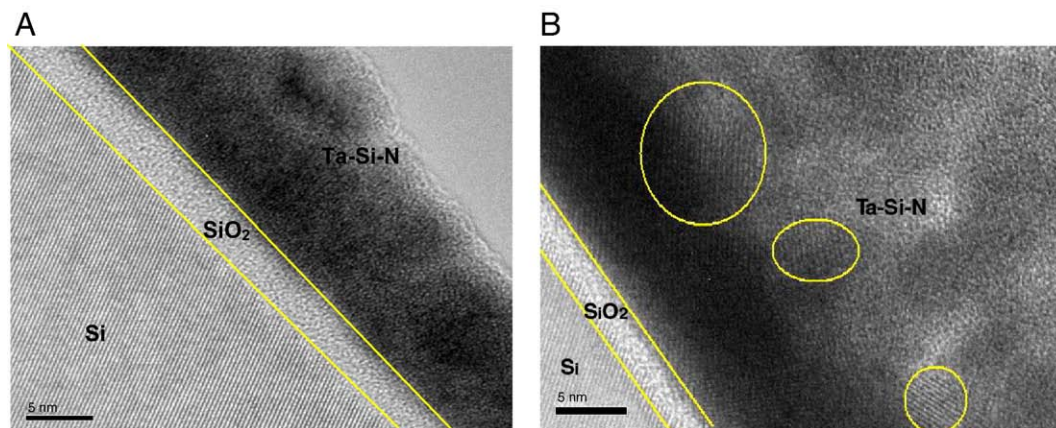


Fig. 3. HRTEM image of N8.5 film annealed for 60 min (A) at 800 °C and (B) at 900 °C.

References

- [1] S. Veprek, S. Reiprich, *Thin Solid Films* 268 (1995) 64.
- [2] S. Veprek, P. Nesladek, A. Niederhofer, F. Glatz, M. Jilek, M. Sima, *Surf. Coat. Technol.* 108–109 (1998) 138.
- [3] C.S. Sandu, R. Sanjines, F. Medjani, *Surf. Coat. Technol.* 202 (2008) 2278.
- [4] J.F. Wang, Z.X. Song, K.W. Xu, *Surf. Coat. Technol.* 201 (2007) 4931.
- [5] S. Veprek, A.S. Argon, R.F. Zhang, *Philos. Mag. Lett.* 87 (2007) 955.
- [6] S. Veprek, M.G.J. Veprek-Heijman, R.F. Zhang, *J. Phys. Chem. Solids* 68 (2007) 1161.
- [7] F. Kauffmann, B. Ji, G. Dehm, H. Gao, E. Arzt, *Scr. Mater.* 52 (2005) 1269.
- [8] Y.C. Ee, Z. Chen, S.B. Law, S. Xu, *Thin Solid Films* 504 (2006) 218.
- [9] Y.C. Ee, J.S. Juneja, P.I. Wang, T.M. Lu, H. Bakhru, L. Chan, S.B. Law, C. Yong, Z. Chen, S. Xu, *J. Electrochem. Soc.* 153 (2006) G470.
- [10] Y.C. Ee, Z. Chen, T.M. Lu, Z.L. Dong, S.B. Law, *Electrochem. Solid-State Lett.* 9 (2006) G100.
- [11] L.W. Lai, *J. Appl. Phys.* 94 (2003) 5396.
- [12] R. Hubner, M. Hecker, N. Mattern, A. Voss, J. Acker, V. Hoffmann, K. Wetzig, H.J. Engelmann, E. Zschech, H. Heuer, C. Wenzel, *Thin Solid Films* 468 (2004) 183.
- [13] J.O. Olowolafe, J. Li, J.W. Mayer, E.G. Colgan, *Appl. Phys. Lett.* 58 (1991) 469.
- [14] M. Del Re, R. Gouttebaron, J.P. Dauchot, P. Leclère, G. Terwagne, M. Hecq, *Surf. Coat. Technol.* 174–175 (2003) 240.
- [15] Y.C. Ee, J.S. Juneja, P.I. Wang, T.M. Lu, H. Bakhru, L. Chan, S.B. Law, C. Yong, Z. Chen, S. Xu, *J. Electrochem. Soc.* 153 (2006) G470.
- [16] S. Kohli, P.R. McCurdy, C.D. Rithner, P.K. Dorhout, A.M. Dummer, F. Brizuela, C.S. Menoni, *Thin Solid Films* 469–470 (2004) 404.
- [17] P. Aubert, H.J. von Bardeleben, F. Delmotte, J.L. Cantin, M.C. Hugon, *Phys. Rev. B* 59 (1999) 10677.
- [18] J.A. Wilks, N.P. Magtoto, J.A. Kelber, V. Arunachalam, *Appl. Surf. Sci.* 253 (2007) 6176.
- [19] B.H. Hwang, *J. Phys., D, Appl. Phys.* 34 (2001) 2469.